Hybrid Nanomaterials

Deutsche Ausgabe: DOI: 10.1002/ange.201603852
Internationale Ausgabe: DOI: 10.1002/anie.201603852

Unusual Formation of CoSe@carbon Nanoboxes, which have an Inhomogeneous Shell, for Efficient Lithium Storage

*Han Hu, Jintao Zhang, Buyuan Guan, and Xiong Wen (David) Lou**

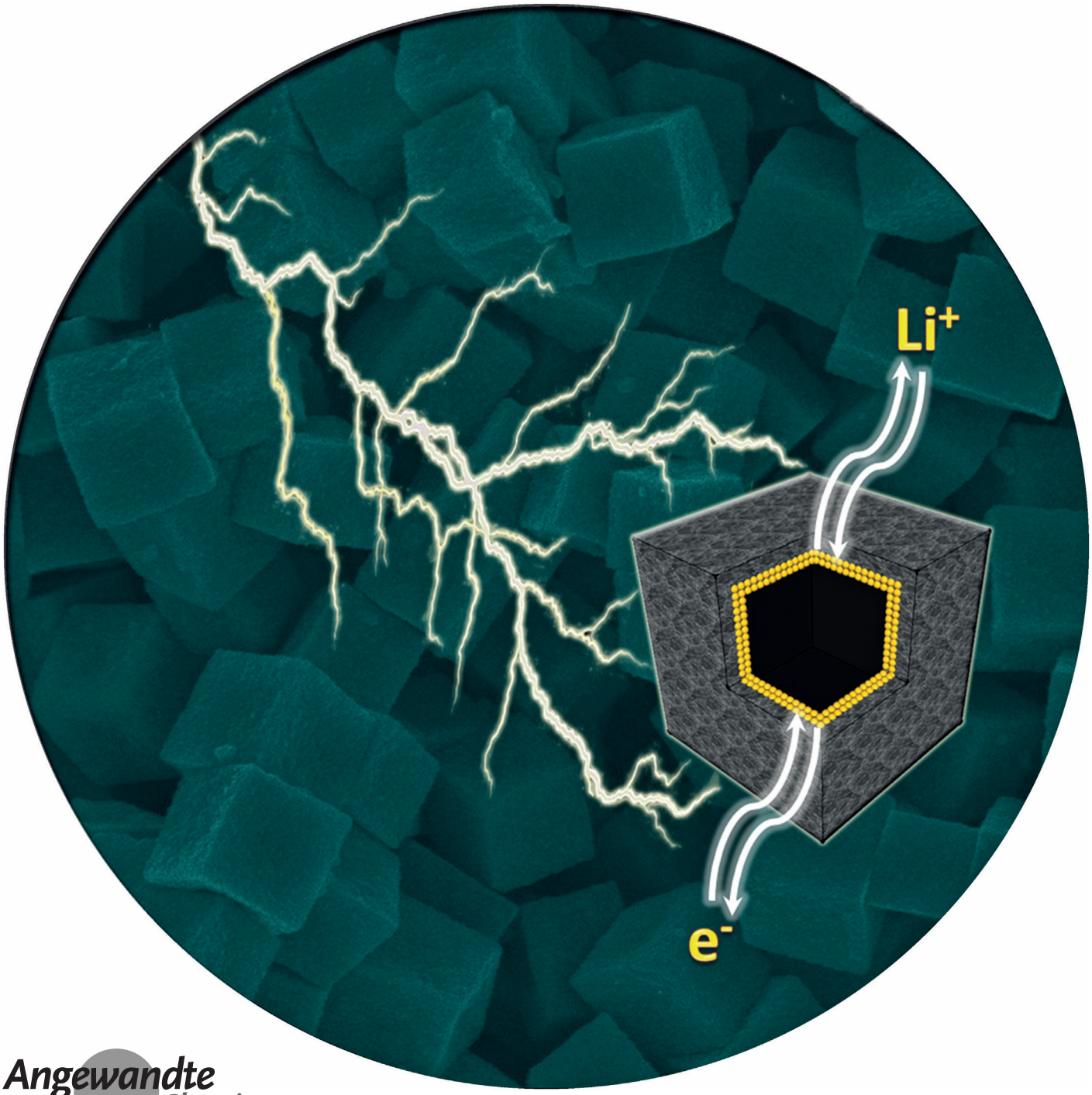

Abstract: *Hybrid hollow nanostructures with tailored shell architectures are attractive for electrochemical energy storage applications. Starting with metal–organic frameworks (MOFs), we demonstrate a facile formation of hybrid nanoboxes with complex shell architecture where a CoSe-enriched inner shell is intimately confined within a carbon-enriched outer shell (denoted as CoSe@carbon nanoboxes). The synthesis is realized through manipulation of the template-engaged reaction between Co-based zeolitic imidazolate framework (ZIF-67) nanocubes and Se powder at elevated temperatures. By virtue of the structural and compositional features, these unique CoSe@carbon nanoboxes manifest excellent lithium-storage performance in terms of high specific capacity, exceptional rate capability, excellent cycling stability, and high initial Coulombic efficiency.*

Rechargeable lithium-ion batteries (LIBs) have been the predominant power source for portable electronics and will be of vital importance for the deployment and application of renewable and sustainable energy sources.[1–4] To meet the requirements of these emerging large-scale energy storage applications, it is urgently required to develop high-energy density LIBs based on advanced anode materials. Currently, graphite based anodes are used in most commercial LIBs with a low theoretical capacity of only 372 $mAh\,g^{-1}$.[3,5,6] As an important family of functional materials, transition-metal chalcogenides (TMCs) can in principle give much higher lithium-storage capacity through conversion reactions, in addition to several other advantages, such as wide availability and intrinsically enhanced safety.[7–10] However, the huge volume variation of TMCs during the lithium insertion/extraction processes causes rapid capacity fading, while their low electrical conductivity usually results in poor rate capability.[7,9] Therefore, the electrochemical performance of these compounds has to be improved through structural and compositional engineering for real applications.[5,9–11]

One possible solution to address these issues is to design and synthesize complex structures with nanostructured active species confined within hollow carbon shells.[12–15] In such nanostructures, the void space can accommodate the huge volume change of TMCs, while the confinement effect of carbon shells prevents their pulverization and aggregation during lithiation/delithiation processes.[16] On the other hand, the TMCs with rationally engineered nanostructures coupled with the surrounded conductive matrix provide facilitated pathway for charge transport.[7] As a result, the TMC anodes based on the aforementioned design rationales are supposed to deliver enhanced lithium storage performance. A wealth of related hybrid structures, including graphene nanosheet-wrapped $CoSe_2$ composites,[17] MoS_2 nanoplate@graphene nanocables,[18] and carbon coated CoS_2 nanosheet-assembled hollow spheres with tunable voids,[19] have been demonstrated to exhibit superior lithium storage performance. In addition, manipulating the crystallinity of the carbon shells and their coupling effects with the TMCs may bring additional possibilities to boost the electrochemical performance of electrode materials.[20] For example, the direct nanocoating of active species with amorphous carbon usually leads to a higher initial Coulombic efficiency (ICE).[6,20–23] However, the synthesis of such hybrid hollow structures which rationally integrate all these features remains as a great challenge due to the difficulties in simultaneously manipulating materials with distinct physical/chemical properties in a designed manner.

With perfectly assembled metal ions and organic ligands in the crystal lattice, metal–organic frameworks (MOFs) provide great advantages for constructing hybrid nanostructures made of TMC and carbon owing to their unique chemical reactivity and thermal behavior.[24,25] A myriad of such hybrid structures have been synthesized by using MOFs as precursors and/or templates.[7,26] Herein, we report a designed formation of novel hybrid nanoboxes with a CoSe-enriched inner shell intimately confined within a carbon-enriched outer shell (denoted as CoSe@carbon nanoboxes) by a facile MOFs-engaged strategy. When evaluated as an anode material for LIBs, the CoSe@carbon nanoboxes manifest high specific capacity, exceptional rate capability, and long-term cycling stability. Moreover, this hybrid structure shows a small irreversible capacity loss during the first discharge/charge cycle with a high ICE of 78.3%.

The synthesis procedure of the CoSe@carbon nanoboxes is schematically illustrated in Figure 1. Uniform Co-based zeolitic imidazolate framework (ZIF-67) nanocubes are facilely synthesized by a cetyltrimethylammonium bromide (CTAB)-mediated method.[27] The collected ZIF-67 nanocubes are uniformly mixed with Se powder, which is then annealed at 350°C in nitrogen atmosphere. During this process, nanoboxes with a $CoSe_2$ nanoparticles-embedded

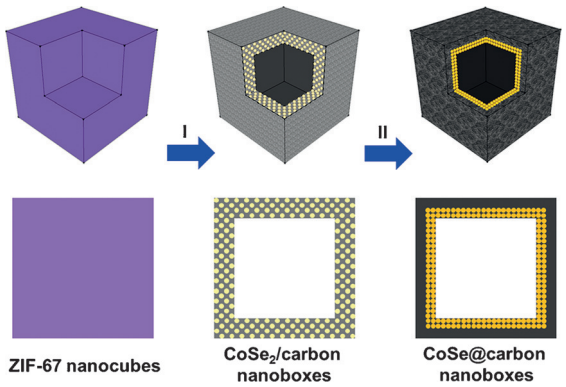

Figure 1. Schematic illustration of the formation process of CoSe@carbon nanoboxes: I) formation of $CoSe_2$/carbon nanoboxes by annealing ZIF-67 nanocubes and Se powder at 350°C for 2 h in a nitrogen atmosphere and II) the growth of CoSe@carbon nanoboxes by further annealing $CoSe_2$/carbon nanoboxes at 600°C for another 2 h in a nitrogen atmosphere.

[*] Dr. H. Hu, J. T. Zhang, Dr. B. Y. Guan, Prof. X. W. Lou
School of Chemical and Biomedical Engineering
Nanyang Technological University
62 Nanyang Drive, Singapore, 637459 (Singapore)
E-mail: xwlou@ntu.edu.sg
Homepage: http://www.ntu.edu.sg/home/xwlou/

Supporting information for this article can be found under: http://dx.doi.org/10.1002/anie.201603852.

carbon shell (denoted as $CoSe_2$/carbon nanoboxes) are formed mainly because of the different diffusion rates of cobalt and selenium.[28] After further annealing the $CoSe_2$/carbon nanoboxes at 600 °C in nitrogen atmosphere, the $CoSe_2$ nanoparticles can be chemically converted into CoSe nanoparticles,[29] which further accumulate in the inner shell of the nanoboxes. As a result, unique nanoboxes with a CoSe-enriched inner shell intimately confined within a carbon-enriched outer shell are eventually obtained.

The materials at different stages are thoroughly characterized and analyzed by powder X-ray diffraction (XRD), energy-dispersive X-ray spectroscopy (EDX), Raman spectroscopy, field-emission scanning electron microscopy (FESEM), and transmission electron microscopy (TEM). The typical diffraction peaks of (011), (112), (222), and (134) in the XRD pattern (Figure S1a in the Supporting Information) can be well indexed to phase-pure ZIF-67, which is in congruent with previous reports.[30–33] The panoramic FESEM image (Figure S1b) reveals that the as-formed ZIF-67 particles consist exclusively of uniform nanocubes with a size of about 730 nm. FESEM image under higher magnification (Figure S1c) reveals that the ZIF-67 nanocubes have rather smooth surfaces over the whole particle, while the TEM characterization (Figure S1d) verifies the solid nature. After treating with Se at 350 °C in nitrogen atmosphere for 2 h, the diffraction peaks in the XRD pattern can be attributed to the $CoSe_2$ phase (Figure S2a). The EDX spectrum shows a Se/Co atomic ratio of 2.14 (Figure S2b), providing further evidence of forming $CoSe_2$. The carbon matrix is determined to be amorphous, revealed by a large I_D/I_G ratio of 2.30 (area ratio) in the Raman spectrum (Figure S2c). FESEM examinations (Figure 2a,b, and Figure S2d in the Supporting Information) indicate that these uniform particles still show the cubic morphology but exhibit rough surfaces with densely embedded $CoSe_2$ nanoparticles. The hollow interior of these $CoSe_2$/carbon nanoboxes is unambiguously elucidated by the sharp contrast between the shell and the inner cavity under TEM observations (Figure 2c,d). The thickness of the shells is around 150 nm (Figure 2d) and the amorphous carbon-coated $CoSe_2$ nanoparticles (Figure S2e) are uniformly distributed throughout the whole shell. The evolution of the hollow interior can be described by a bulk version of the Kirkendall effect.[28] Specifically, during the reaction process which takes place mainly near the surface region, selenium slowly diffuses inward while cobalt species flows outward at a higher rate. The different diffusion rates of selenium and cobalt would be balanced by the formation of the hollow interior, thus giving rise to the $CoSe_2$/carbon nanoboxes.

Upon further annealing at 600 °C in inert atmosphere, the $CoSe_2$ nanoparticles are chemically converted into nanostructured CoSe as evidenced from the XRD pattern and EDX spectrum (Figure S3a,b), while the carbon matrix still remains amorphous despite the increase of carbonization degree revealed by a decreased I_D/I_G ratio of 1.63 in the Raman spectrum (Figure S3c). From FESEM observation (Figure 3a,b, and from Figure S3d in the Supporting Information), this sample inherits the cubic shape and uniformity from the $CoSe_2$/carbon nanoboxes. Interestingly, TEM observation reveals the inhomogeneous distribution of CoSe nanoparticles. As shown in Figure 3c,d, the dark inner shell suggests a region where the CoSe nanoparticles are concentrated. In contrast, the carbon-enriched outer shell shows a lower contrast. Elemental mapping is also performed to further illustrate the inhomogeneous feature. As shown in Figure 3e–g, the intensity of cobalt and selenium is apparently enhanced in the inner shell of the nanobox, significantly different from that of carbon. Both the inner and outer shells have a similar thickness of around 70 nm (Figure S3e). The evolution of a uniform shell into such an inhomogeneous complex shell structure is quite intriguing, which might be related to the combined effects of the chemical transformation of $CoSe_2$ and the further carbonization of the shell

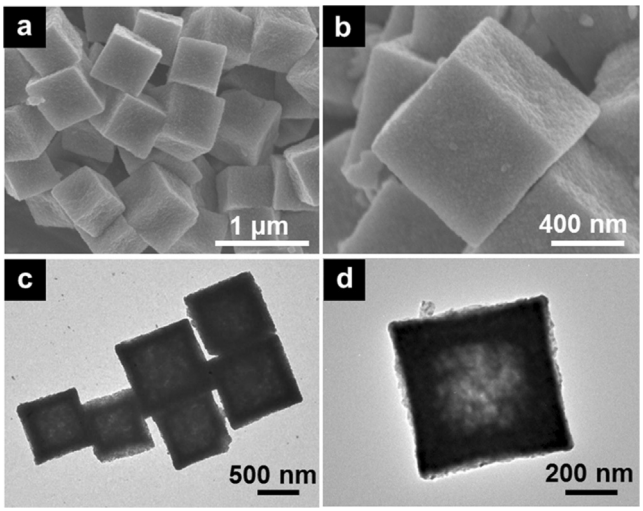

Figure 2. a),b) FESEM images and c),d) TEM images of $CoSe_2$/carbon nanoboxes synthesized by annealing ZIF-67 nanocubes and Se powder at 350 °C for 2 h in a nitrogen atmosphere.

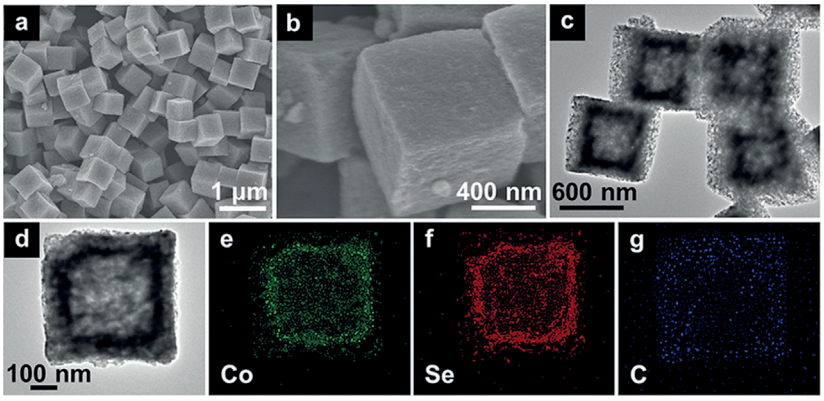

Figure 3. a),b) FESEM images and c),d) TEM images of the CoSe@carbon nanoboxes synthesized by annealing $CoSe_2$/carbon nanoboxes at 600 °C for 2 h in a nitrogen atmosphere. Elemental mapping images of Co (e), Se (f), and C (g) of the individual nanobox shown in (d).

matrix. The high-resolution TEM (HRTEM) analysis (Figure S3 f) shows that the CoSe nanocrystals in the shell are well coated by amorphous carbon. Such a unique structure can provide excellent protection of the active species from migration and pulverization during the repeated discharge/charge processes.[34] The content of the CoSe in the CoSe@carbon nanoboxes is determined by thermogravimetric analysis (TGA; Figure S4) to be about 69 wt%. The nitrogen sorption isotherm (Figure S5) shows that these nanoboxes have a large specific surface area of 110 $m^2 g^{-1}$ as well as a highly porous structure with pore size broadly distributed in the range of 2–20 nm.

The electrochemical properties of these CoSe@carbon nanoboxes are evaluated as an anode material for LIBs. The representative cyclic voltammetry (CV) curve of the 1st cycle within a potential range of 0.01–3.0 V versus Li/Li^+ shows a pronounced cathodic peak around 1.1 V and an anodic peak at 2.1 V (Figure S6), which are associated with the lithium insertion and extraction reactions, respectively.[35] From the 2nd cycle onwards, the position of the cathodic peaks shifts to 1.4 V after the structural variation and activation of the electrode materials during the first cycle.[17,36] Besides, the well overlapped CV curves reveal the good reversibility of the electrode materials from then on. Interestingly, the broad cathodic peak around 0.6 V in the 1st cycle, which is usually associated with the inevitable formation of a solid electrolyte interface (SEI) layer,[37] is relatively small, which might lead to a high ICE. The high ICE is then confirmed by the galvanostatic discharge/charge test. As shown in Figure 4a, the first discharge and charge capacities at a current density of 0.2 $A g^{-1}$ are about 1016 and 796 $mAh g^{-1}$, respectively, giving an ICE of 78.3%. This value is superior to that of many related structures reported elsewhere,[7,12,18] which may be associated with the fact that the electroactive CoSe nanoparticles are coated by amorphous carbon.[6,22] The high ICE can be well maintained at higher current densities. When cycled at current densities of 0.5 and 1.0 $A g^{-1}$, the ICE is about 75.3% and 76.2%, respectively (Figure S7). Figure 4b shows the rate performance of the CoSe@carbon nanoboxes. When cycled at current densities of 0.2, 0.5, 1.0, and 2.0 $A g^{-1}$, stable capacities of 787, 755, 722, and 686 $mAh g^{-1}$ respectively can be obtained. The capacity retention is as high as 87% with the 10-fold increase of current density, indicative of the exceptional rate capability. After reducing the current density back to 0.2 $A g^{-1}$, the capacity is slightly increased to 848 $mAh g^{-1}$, which might be attributed to the activation caused by high-rate discharging/charging.[38] The cycling performance has been tested at current densities of 0.2, 0.5, and 1.0 $A g^{-1}$ (Figure 4c). As can be seen, the discharge capacity at a current density of 0.2 $A g^{-1}$ gradually increases from 796 $mAh g^{-1}$ in the 2nd cycle to 860 $mAh g^{-1}$ in the 100th cycle. Such a capacity rise is quite normal for many conversion-type electrode materials mainly because of reversible formation of a polymeric gel-like layer which provides excess capacity through a "pseudo-capacitance-type behavior".[39] The capacity retention is very good even at higher current densities. When cycled at a current density of 0.5 $A g^{-1}$, a high capacity of 711 $mAh g^{-1}$ can be delivered in the 100th cycle, corresponding to 94.5% of the 2nd cycle discharge capacity. With further increase of current density to 1.0 $A g^{-1}$, the capacity can still be as high as 660 $mAh g^{-1}$ after 100 cycles, corresponding to 91.6% of the 2nd cycle discharge capacity. The superior cycling stability is likely related to the excellent structural stability of the CoSe@carbon nanoboxes. From the post-mortem study (Figure S8), the structure of the CoSe@carbon nanoboxes is well retained after discharging/charging for 100 cycles at a current density of 1.0 $A g^{-1}$. The lithium storage performance of the CoSe@carbon nanoboxes has been further compared with that of the $CoSe_2$/carbon nanoboxes (Figure S9). The discharge capacity of the $CoSe_2$/carbon nanoboxes decays drastically from 623 $mAh g^{-1}$ in the 2nd cycle to only 254 $mAh g^{-1}$ in the 100th cycle at a current density of 1.0 $A g^{-1}$. In addition, the CoSe@carbon nanoboxes also outperform many transition-metal selenide-based anodes reported elsewhere (Figure S10 and Table S1).

The excellent lithium-storage performance of the CoSe@carbon nanoboxes can be attributed to the advantageous nanoarchitectures. Specifically, the hollow interior of the CoSe@carbon nanoboxes can buffer the stress induced by CoSe-involved conversion reactions during the repeated lithiation/delithiation processes. The CoSe nanoparticles are very well protected by the outer carbon layer, which can not

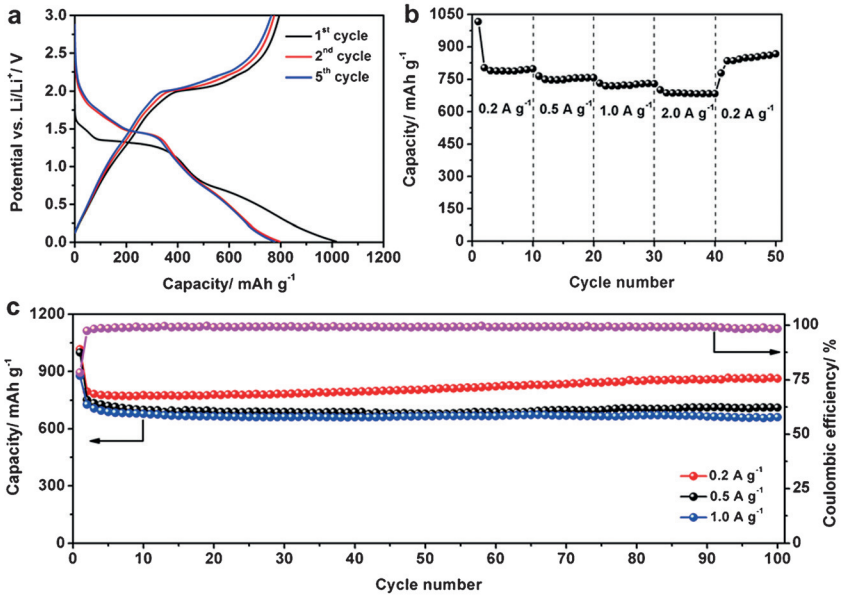

Figure 4. Electrochemical performance of the CoSe@carbon nanoboxes. a) Discharge/charge voltage profiles at a current density of 0.2 $A g^{-1}$, b) rate performance at current densities ranging from 0.2 to 2.0 $A g^{-1}$, and c) cycling performance at current densities of 0.2, 0.5, 1.0 $A g^{-1}$ and the Coulombic efficiency at a current density of 0.2 $A g^{-1}$.

only prevent their pulverization and shedding but also leads to high ICE. The overall porous carbon matrix provides pathways for charge transport thus permitting the effective lithium insertion/extraction even at high current densities.

In summary, we report a template-induced formation of CoSe@carbon nanoboxes through the template-induced reaction between ZIF-67 nanocubes and Se powder at elevated temperature. In the synthesis, $CoSe_2$/carbon nanoboxes are first formed with $CoSe_2$ nanoparticles uniformly distributed throughout the carbon shell at a lower annealing temperature. After further annealing at a higher temperature, the $CoSe_2$ nanoparticles are chemically converted into CoSe nanoparticles leading to the formation of the CoSe@carbon nanoboxes. Benefiting from the structural and compositional features, the CoSe@carbon nanoboxes show excellent lithium-storage performance in terms of high capacity, exceptional rate performance, excellent cyclability, and high initial Coulombic efficiency.

Keywords: CoSe · hybrid structures · lithium-ion batteries · nanoboxes · ZIF-67

How to cite: *Angew. Chem. Int. Ed.* **2016**, *55*, 9514–9518
Angew. Chem. **2016**, *128*, 9666–9670

[1] M. Armand, J. M. Tarascon, *Nature* **2008**, *451*, 652.
[2] H. Liu, W. Li, D. K. Shen, D. Y. Zhao, G. X. Wang, *J. Am. Chem. Soc.* **2015**, *137*, 13161.
[3] P. G. Bruce, B. Scrosati, J. M. Tarascon, *Angew. Chem. Int. Ed.* **2008**, *47*, 2930; *Angew. Chem.* **2008**, *120*, 2972.
[4] M. V. Reddy, G. V. S. Rao, B. V. R. Chowdari, *Chem. Rev.* **2013**, *113*, 5364.
[5] Z. Y. Wang, L. Zhou, X. W. Lou, *Adv. Mater.* **2012**, *24*, 1903.
[6] J. C. Guo, Z. C. Yang, L. A. Archer, *J. Mater. Chem. A* **2013**, *1*, 8710.
[7] R. B. Wu, D. P. Wang, X. H. Rui, B. Liu, K. Zhou, A. W. K. Law, Q. Y. Yan, J. Wei, Z. Chen, *Adv. Mater.* **2015**, *27*, 3038.
[8] S. H. Choi, Y. C. Kang, *Small* **2014**, *10*, 474.
[9] X. Y. Yu, H. Hu, Y. W. Wang, H. Y. Chen, X. W. Lou, *Angew. Chem. Int. Ed.* **2015**, *54*, 7395; *Angew. Chem.* **2015**, *127*, 7503.
[10] C. B. Zhu, X. K. Mu, P. A. van Aken, Y. Yu, J. Maier, *Angew. Chem. Int. Ed.* **2014**, *53*, 2152; *Angew. Chem.* **2014**, *126*, 2184.
[11] H. Hu, L. Yu, X. H. Gao, Z. Lin, X. W. Lou, *Energy Environ. Sci.* **2015**, *8*, 1480.
[12] Z. Liu, X.-Y. Yu, U. Paik, *Adv. Energy Mater.* **2016**, *6*, 1502318.
[13] D. Li, H. Wang, H. K. Liu, Z. Guo, *Adv. Energy Mater.* **2016**, *6*, 1501666.
[14] H. W. Zhang, L. Zhou, O. Noonan, D. J. Martin, A. K. Whittaker, C. Z. Yu, *Adv. Funct. Mater.* **2014**, *24*, 4337.
[15] W.-M. Zhang, J.-S. Hu, Y.-G. Guo, S.-F. Zheng, L.-S. Zhong, W.-G. Song, L.-J. Wan, *Adv. Mater.* **2008**, *20*, 1160.
[16] X.-Y. Yu, L. Yu, X. W. Lou, *Adv. Energy Mater.* **2016**, *6*, 1501333.
[17] Z. P. Li, H. T. Xue, J. Q. Wang, Y. B. Tang, C. S. Lee, S. R. Yang, *ChemElectroChem* **2015**, *2*, 1682.
[18] D. B. Kong, H. Y. He, Q. Song, B. Wang, W. Lv, Q. H. Yang, L. J. Zhi, *Energy Environ. Sci.* **2014**, *7*, 3320.
[19] S. J. Peng, L. L. Li, S. G. Mhaisalkar, M. Srinivasan, S. Ramakrishna, Q. Y. Yan, *ChemSusChem* **2014**, *7*, 2212.
[20] N. Nitta, F. X. Wu, J. T. Lee, G. Yushin, *Mater. Today* **2015**, *18*, 252.
[21] S. H. Ng, J. Wang, D. Wexler, S. Y. Chew, H. K. Liu, *J. Phys. Chem. C* **2007**, *111*, 11131.
[22] Z. Tan, Z. H. Sun, H. H. Wang, Q. Guo, D. S. Su, *J. Mater. Chem. A* **2013**, *1*, 9462.
[23] J. C. Guo, Q. Liu, C. S. Wang, M. R. Zachariah, *Adv. Funct. Mater.* **2012**, *22*, 803.
[24] J. K. Sun, Q. Xu, *Energy Environ. Sci.* **2014**, *7*, 2071.
[25] J. Tang, R. R. Salunkhe, J. Liu, N. L. Torad, M. Imura, S. Furukawa, Y. Yamauchi, *J. Am. Chem. Soc.* **2015**, *137*, 1572.
[26] H. Hu, L. Han, M. Yu, Z. Wang, X. W. Lou, *Energy Environ. Sci.* **2016**, *9*, 107.
[27] H. Hu, B. Y. Guan, X. W. Lou, *Chem* **2016**, accepted.
[28] Y. D. Yin, R. M. Rioux, C. K. Erdonmez, S. Hughes, G. A. Somorjai, A. P. Alivisatos, *Science* **2004**, *304*, 711.
[29] H. X. Zhang, B. Yang, X. L. Wu, Z. J. Li, L. C. Lei, X. W. Zhang, *ACS Appl. Mater. Interfaces* **2015**, *7*, 1772.
[30] H. Hu, B. Y. Guan, B. Y. Xia, X. W. Lou, *J. Am. Chem. Soc.* **2015**, *137*, 5590.
[31] B. L. Chen, Z. X. Yang, Y. Q. Zhu, Y. D. Xia, *J. Mater. Chem. A* **2014**, *2*, 16811.
[32] Z. Jiang, Z. P. Li, Z. H. Qin, H. Y. Sun, X. L. Jiao, D. R. Chen, *Nanoscale* **2013**, *5*, 11770.
[33] D. B. Yu, L. Ge, B. Wu, L. Wu, H. T. Wang, T. W. Xu, *J. Mater. Chem. A* **2015**, *3*, 16688.
[34] H. Q. Li, H. S. Zhou, *Chem. Commun.* **2012**, *48*, 1201.
[35] D. H. Wei, J. W. Liang, Y. C. Zhu, L. Hu, K. L. Zhang, J. J. Zhang, Z. Q. Yuan, Y. T. Qian, *Electrochem. Commun.* **2014**, *38*, 124.
[36] G. Huang, F. F. Zhang, X. C. Du, Y. L. Qin, D. M. Yin, L. M. Wang, *ACS Nano* **2015**, *9*, 1592.
[37] M. Gauthier, T. J. Carney, A. Grimaud, L. Giordano, N. Pour, H. H. Chang, D. P. Fenning, S. F. Lux, O. Paschos, C. Bauer, F. Magia, S. Lupart, P. Lamp, Y. Shao-Horn, *J. Phys. Chem. Lett.* **2015**, *6*, 4653.
[38] Z. Y. Wang, D. Y. Luan, S. Madhavi, Y. Hu, X. W. Lou, *Energy Environ. Sci.* **2012**, *5*, 5252.
[39] S. Laruelle, S. Grugeon, P. Poizot, M. Dolle, L. Dupont, J. M. Tarascon, *J. Electrochem. Soc.* **2002**, *149*, A627.

Received: April 20, 2016
Published online: May 30, 2016

